Nonlinear Dyn (2018) 94:807–826
https://doi.org/10.1007/s11071-018-4395-7

ORIGINAL PAPER

Mixed-mode oscillations and bifurcation analysis in a pituitary model

Feibiao Zhan · Shenquan Liu · Xiaohan Zhang · Jing Wang · Bo Lu

Received: 16 January 2018 / Accepted: 25 May 2018 / Published online: 5 September 2018

Abstract Bursting is an intrinsically electrical activity in excitable cells such as endocrine cells and many types of neurons. Our purpose is to recognize the pituitary model from a new perspective and provide guidance for its further improvement by exploring the mechanism of bursting generation and its dynamic behavior. The technique of slow–fast dynamics analysis is very helpful when analyzing two subsystems that vary significantly in time scale. Based on the original model, A-type potassium channels and BK-type potassium channels are added simultaneously to the system. And its dynamical property differs from merely adding a fast potassium ion channel (A-type or BK-type). We acquire a deeper understanding for the novel bursting pattern (pseudo-plateau) from discussing the original system to considering bifurcation analysis to the whole system. We mainly explore the existence of mixed-mode oscillations (MMOs) in the improved pituitary model and its bifurcation behaviors via using geometric singular perturbation theory and slow–fast dynamics analysis, respectively. The result we obtained is very helpful in explaining mathematical mechanisms and improving the pituitary model.

Keywords Slow–fast dynamics · Mixed-mode oscillations · Bogdanov–Takens bifurcation · Lyapunov coefficient · Pituitary model

F. Zhan · S. Liu (✉) · X. Zhang
School of Mathematics, South China University of Technology, Guangzhou 510640, China
e-mail: mashqliu@scut.edu.cn

J. Wang
School of Applied Mathematics, Guangdong University of Technology, Guangzhou 510520, China
e-mail: wangjing901225@gmail.com

B. Lu
School of Mathematics and Science, Henan Institute of Science and Technology, Xinxiang 453003, China
e-mail: cheersnow@163.com

1 Introduction

Bursting pattern of electrical activity is characterized by episodes of a depolarized spiking (active phase) followed by a hyperpolarized quiescence (silent phase). These bursting oscillations are closely related to physiological significance such as bursting pattern may mean a higher level of neurotransmitter and hormone secretion than tonic spiking [1,2], and this mechanism has become the focus of mathematical exploration and analysis. Many hormone-secreting cell-types in the anterior pituitary gland exhibit the pseudo-plateau bursting pattern, and they have been established on their own mathematical model, such as lactotroph [3,4], which secrete prolactin, somatotroph [5], and corticotroph [6–8], which secrete adrenocorticotrophic hormone. Pseudo-plateau bursting is different from many types of neuron models with plateau (square-wave) bursting, as reported in [9]. Bursting pattern is diverse both in the external presentation and in the internal ion mechanism, and considerable advancement has been made to tie them together [10–14]. Recently, the rela-

tionship between bifurcation mechanism and bursting pattern is discussed in [15–17].

In many neuron models, dynamical behaviors of bursting pattern have been explored using a variety of methods such as bifurcation theory [18,19], adding time delay [20,21], increasing electromagnetic radiation [22–25], geometric singular perturbation theory (GSPT)[26–30] and so on. Similarly, many pituitary models can be implemented using these methods as a tool to explore their intrinsic dynamics. One of these, the lactotroph model, has abundantly potential dynamic behaviors, and it was researched in [31–34] using geometric singular perturbation theory and slow–fast dynamics analysis. However, there is a little information on detailed bifurcation analysis and specifically theoretical illustration of MMOs. One of the purposes of this paper is to enhance the result that lacks detailed calculation. Therefore, we attempt to explore some properties of different bursting oscillations and also analyze related bifurcation to further understand bursting modes in the lactotroph model. Furthermore, we find that the MMOs of signature 1^s exist, and some bursting patterns are illustrated using slow–fast dynamics in detail. And one fast variable analysis complements the information that is not obtained from one slow variable analysis. Moreover, we investigate one-parameter bifurcation and determine the stability of the Hopf bifurcation via calculating the first Lyapunov coefficient to improve the understanding of bursting and spiking. In addition, we also explicate two-parameter bifurcation analysis in the $(g_{\mathrm{bk}}, g_{\mathrm{sk}})$ phase plane and analyze the Bogdanov–Takens bifurcation. It is not easy that a saddle homoclinic bifurcation curve was discovered near the Bogdanov–Takens bifurcation point.

The rest of this paper is organized as follows. Section 2 describes the lactotroph model and explicates the theoretical tools that we use in simulation. We illustrate dynamics of MMOs in Sects. 3.1 and 3.2. In Sect. 3.3, we research the bursting pattern and compare it with the first two sections. Section 4 explores behavior of the Hopf bifurcation point. In Sect. 5, we consider codimension-two bifurcation of the whole system in the $(g_{\mathrm{bk}}, g_{\mathrm{sk}})$ phase plane and exhibit the Bogdanov–Takens bifurcation. Finally, we have a discussion with the conclusion in Sect. 6.

2 Model and methods

We improve a single-compartment model [3] that was developed by modifying previous model for the pituitary lactotroph. We explore the model that contains calcium ion current, delayed rectifier potassium current, calcium-activated potassium current, BK-type potassium current and A-type potassium current. The four variables are the membrane voltage V, the activated gating channel (n) of the delayed rectifier potassium current, the cytosolic-free concentration [Ca] and the inactivated channel (h) of the A-typed potassium current, respectively. The four differential equations are described as follows:

$$C_{\mathrm{m}}\frac{\mathrm{d}V}{\mathrm{d}t} = -(I_{\mathrm{Ca}} + I_{\mathrm{K}} + I_{\mathrm{SK}} + I_{\mathrm{BK}} + I_A), \tag{1}$$

$$\tau_n\frac{\mathrm{d}n}{\mathrm{d}t} = \lambda(n_\infty(V) - n), \tag{2}$$

$$\frac{\mathrm{d}[\mathrm{Ca}]}{\mathrm{d}t} = -f_c(\alpha I_{\mathrm{Ca}} + k_c[\mathrm{Ca}]), \tag{3}$$

$$\tau_h\frac{\mathrm{d}h}{\mathrm{d}t} = (h_\infty(V) - h). \tag{4}$$

where I_{Ca}, I_{K}, I_{SK}, I_{BK} and I_A are inward calcium ion current, delayed rectifier type current, calcium-activated potassium ion current, fast potassium current and A-type current, respectively. The specific expression of ion currents are described by

$$I_{\mathrm{Ca}} = g_{\mathrm{ca}}m_\infty(V)(V - V_{\mathrm{Ca}}),$$
$$I_{\mathrm{K}} = g_{\mathrm{k}}n(V - V_{\mathrm{K}}),$$
$$I_{\mathrm{SK}} = g_{\mathrm{sk}}s_\infty([\mathrm{Ca}])(V - V_{\mathrm{K}}),$$
$$I_{\mathrm{BK}} = g_{\mathrm{bk}}f_\infty(V)(V - V_{\mathrm{K}}),$$
$$I_A = g_{\mathrm{a}}a_\infty(V)h(V - V_{\mathrm{Ca}}).$$

Steady-state functions are given by

$$x_\infty(V) = \frac{1}{\{1 + \exp[(v_x - V)/s_x]\}},$$
$$for\ x = m, n, h, f, a,$$
$$s_\infty([\mathrm{Ca}]) = \frac{[\mathrm{Ca}]^2}{\{[\mathrm{Ca}]^2 + {k_s}^2\}}.$$

Corresponding system parameters are: membrane capacitance C_{m} (pF), time constant τ_n, τ_h, reversal potential V_{Ca} (calcium), V_{K} (potassium), maximal conductance g_{ca}, g_{k}, g_{sk}, g_{bk}, g_{a} and related parameter for steady-state functions v_x, $s_x(x = m, n, h, f, a)$. In addition to some variables, other fixed parameters throughout the paper are given in Table 1.

We have an extended dynamical understanding of the lactotroph cell model from the use of geometric singular perturbation theory for the system consists of Eqs. (1)–(3) to the application of slow–fast dynamics analysis and bifurcation theory for the whole system. MATCONT is a continuation package in MATLAB, which is a powerful nonlinear dynamics bifurcation and chaos analysis software. For example, it can explore curves of equilibria, fold bifurcation point, Hopf bifurcation point, branch point, limit point bifurcation of cycles (LPC), period doubling bifurcation point and so on in codimension-one bifurcation, and in codimension-two bifurcation, it can compute cusp bifurcation point, Bogdanov–Takens bifurcation point, generalized Hopf bifurcation point, fold curve, Hopf curve, period doubling curve, LPC curve and so on. Of course, only a small part of its functionality is used here. We are using MATLAB and MATCONT software package [35,36] for all numerical calculation and graphic rendering, and adopt fourth-order Runge–Kutta algorithm in all of simulation and calculation.

3 Dynamics analysis

3.1 MMOs in the lactotroph model with three differential equations

Let $V = k_v v$, $t = k_t \tau$, then the system consists of Eqs. (1)–(3) transforms to

$$\begin{aligned}
\frac{\mathrm{d}v}{\mathrm{d}\tau} &= \frac{g_{\max} k_t}{C_{\mathrm{m}}}[-\overline{g}_{\mathrm{ca}} m_\infty(v)(v - V_{\mathrm{Ca}}) - \overline{g}_{\mathrm{k}} n(v - V_{\mathrm{k}}) \\
&\quad - \overline{g}_{\mathrm{sk}} s_\infty([\mathrm{Ca}])(v - V_{\mathrm{K}}) - \overline{g}_{\mathrm{bk}} f_\infty(v)(v - V_{\mathrm{K}})], \\
\frac{\mathrm{d}n}{\mathrm{d}\tau} &= \frac{k_t \lambda\,(n_\infty - n)}{\tau_n}, \\
\frac{\mathrm{d}[\mathrm{Ca}]}{\mathrm{d}\tau} &= -k_t f_c \left(\alpha \overline{g}_{\mathrm{ca}} m_\infty(v)(v - V_{\mathrm{Ca}}) + k_c[\mathrm{Ca}]\right),
\end{aligned}$$

where $g_{\max} = 100$ nS, $k_v = 1$ mv, $k_t = 1$ ms, $\overline{g}_i = g_i / g_{\max}$ and i represents ca,k,sk,bk. We can obtain the dimensionless system Eqs. (5)–(7) by setting

$$\begin{aligned}
&\varepsilon \triangleq C_{\mathrm{m}}/(g_{\max} k_t) \ll 1. \\
&\quad \varepsilon \frac{\mathrm{d}v}{\mathrm{d}\tau} = -\overline{g}_{\mathrm{ca}} m_\infty(v)(v - V_{\mathrm{Ca}}) - \overline{g}_{\mathrm{k}} n(v - V_{\mathrm{K}}) \\
&\quad - \overline{g}_{\mathrm{sk}} s_\infty([\mathrm{Ca}])(v - V_{\mathrm{K}}) - \overline{g}_{\mathrm{bk}} f_\infty(v)(v - V_{\mathrm{K}}) \\
&\quad \triangleq f\,(v, n, [\mathrm{Ca}])\,, \qquad (5) \\
&\frac{\mathrm{d}n}{\mathrm{d}\tau} = \frac{\lambda\,(n_\infty - n)}{\tau_n} \triangleq g_1\,(v, n)\,, \qquad (6) \\
&\frac{\mathrm{d}[\mathrm{Ca}]}{\mathrm{d}\tau} = -f_c \left(\alpha \overline{g}_{\mathrm{ca}} m_\infty(v)(v - V_{\mathrm{Ca}}) + k_c[\mathrm{Ca}]\right) \\
&\quad \triangleq g_2\,(v, [\mathrm{Ca}])\,. \qquad (7)
\end{aligned}$$

It is a singular perturbation system; ε is the perturbation parameter. The model variable V is a fast kinetic variable, while $(n, [\mathrm{Ca}])$ is slow kinetic variable. We make the timescale transformation $\tau = \varepsilon t_1$, and letting $\varepsilon \to 0$, the system will be transformed into a layer problem as the following:

$$\frac{\mathrm{d}v}{\mathrm{d}\tau} = f\,(v, n, [\mathrm{Ca}])\,, \quad \frac{\mathrm{d}n}{\mathrm{d}\tau} = 0, \quad \frac{\mathrm{d}[\mathrm{Ca}]}{\mathrm{d}\tau} = 0.$$

Solutions of the layer system are called fast fibers.

Statement 1 The critical manifold S_0 of the system consists of Eqs. (5)–(7) is a locally folded surface.

We can show that $f(v, n, [\mathrm{Ca}])$ and $f_v(v, n, [\mathrm{Ca}])$ (partial derivative of $f(v, n, [\mathrm{Ca}])$ to v) are continuous bounded functions in the closed regions $I = [-80, 10] \times [0, 0.3] \times [0.2, 0.4]$. By the intermediate value theorem on continuous functions, we can know that the null surface of $f_v(v, n, [\mathrm{Ca}])$ is existent. The critical manifold is consisted of equilibrium points of the fast subsystem, and it is shown as follow: $S_0 = \{(v, n, [\mathrm{Ca}]) : f(v, n, [\mathrm{Ca}]) = 0\}$, that is, S_0 is a folded surface that satisfies the equation.

As shown in Fig. 1a, the locally critical manifold S is the part of S_0 and it satisfies $S = \{(v, n, [\mathrm{Ca}]) \in I,\ f(v, n, [\mathrm{Ca}]) = 0\}$. And $S = {S_a}^+ \cup L^+ \cup S_r \cup L^- \cup {S_a}^-$, where ${S_a}^\pm = \{(v, n, [\mathrm{Ca}]) \in S,\ f_v(v, n, [\mathrm{Ca}]) < 0\}$ are two attracting branches, $S_r = \{(v, n, [\mathrm{Ca}]) \in S,\ f_v(v, n, [\mathrm{Ca}]) > 0\}$ is the repelling branches. $L^\pm = \{(v, n, [\mathrm{Ca}]) \in S,\ f_v(v, n, [\mathrm{Ca}]) = 0,\ f_{vv}(v, n, [\mathrm{Ca}]) \neq 0\}$ are two folded curves.

In Fig. 1b, we can describe two folded curves, which are intersecting curves of the locally critical manifold and the null surface and they are denoted by L^+ and L^-, respectively. Therefore, we can obtain the statement that the global return mechanism is formed in the critical manifold. The trajectory (pink) is resting until it reaches the folded curves L^- along the lower critical manifold. Then the trajectory leave the folded curve L^- along the fast fibers arrive to the upper attracting branch, and reach to the folded curves L^+ along the upper critical manifold, and eventually it returns to the starting point along the fast fibers and exactly through

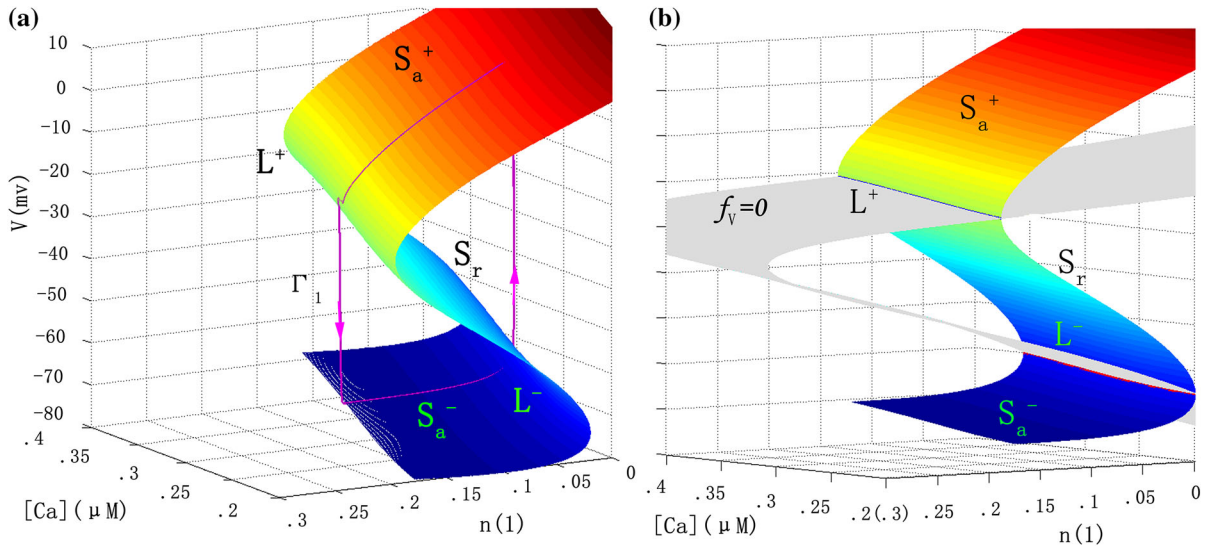

Fig. 1 The critical manifold of system (5)–(7); **a** the superimposed diagram of the trajectory ($C_m = 0.1pF$) and the critical surface; **b** folded curve in the critical manifold. (Color figure online)

the jump point L^+. Repeating the above process, relaxation oscillations can be discovered.

Definition 3.1 [30] Fold point $P_0 \in L^{\pm}$ is called a jump point, if it satisfies the normal switching condition $f_n g_1 + f_{[\mathrm{Ca}]} g_2 \neq 0$.

Definition 3.2 Fold point $P_0 \in L^{\pm}$ is called a folded saddle, folded node and folded focus, if it is not a jump point (is a singular point) and the equilibrium of system Eqs. (6), (7) restricted to S corresponds to saddle, node and focus, respectively.

Statement 2 There exists a folded singular node $P_0 \in L^{\pm}$ in the system consists of Eqs. (5)–(7), which satisfies $f_n g_1 + f_{[\mathrm{Ca}]} g_2 = 0$, and eigenvalues of Jacobian matrix of Eqs. (6), (7) restricted to S at P_0 are: $-9209836.318, -0.1598397647$.

The folded singularities of the system satisfy:

$$f(P_0) = 0, \quad \frac{\partial f}{\partial v}(P_0) = 0, \quad \frac{\partial^2 f}{\partial v^2}(P_0) \neq 0,$$
$$\frac{\partial f}{\partial n}(P_0)\, g_1(P_0) + \frac{\partial f}{\partial [\mathrm{Ca}]}(P_0)\, g_2(P_0) = 0.$$

Let $\varepsilon \to 0$ (Eqs. 5–7), we can give the 2D reduced system (left):

$$\begin{cases} 0 = f(v, n, [\mathrm{Ca}]), \\ \dfrac{\mathrm{d}n}{\mathrm{d}\tau} = g_1(v, n), \\ \dfrac{\mathrm{d}[\mathrm{Ca}]}{\mathrm{d}\tau} = g_2(v, [\mathrm{Ca}]), \end{cases} \Rightarrow \begin{cases} -f_v \dfrac{\mathrm{d}v}{\mathrm{d}\tau} = f_n g_1 + f_{[\mathrm{Ca}]} g_2, \\ \dfrac{\mathrm{d}n}{\mathrm{d}\tau} = g_1(v, n), \\ \dfrac{\mathrm{d}[\mathrm{Ca}]}{\mathrm{d}\tau} = g_2(v, [\mathrm{Ca}]), \end{cases}$$

which depict the flow of reduced problem. Usually, we need to cover a manifold to explain more than a single coordinate chart. Here, the critical manifold is exhibited in Fig. 1, which remind us to use one coordinate chart and we can obtain the projection phase plane of the reduced system

$$\begin{cases} \dfrac{\mathrm{d}v}{\mathrm{d}\tau} = -\dfrac{H_1(v, n, [\mathrm{Ca}])}{H_2(v, n, [\mathrm{Ca}])}, \\ \dfrac{\mathrm{d}[\mathrm{Ca}]}{\mathrm{d}\tau} = -f_c(\alpha \bar{I}_{\mathrm{Ca}} + k_c[\mathrm{Ca}]), \end{cases}$$

restricted to

$$n = -\frac{1}{\bar{g}_{\mathrm{k}}}\left[\bar{g}_{\mathrm{ca}} m_\infty(v)\frac{v - V_{\mathrm{Ca}}}{v - V_{\mathrm{K}}} + \bar{g}_{\mathrm{sk}} s_\infty([\mathrm{Ca}]) + \bar{g}_{\mathrm{bk}} f_\infty(v)\right],$$

where

$$\begin{aligned} H_1(v, n, [\mathrm{Ca}]) &= f_n g_1 + f_{[\mathrm{Ca}]} g_2 \\ &= \bar{g}_{\mathrm{sk}} \dot{s}_\infty([\mathrm{Ca}])[-f_c(\alpha \bar{I}_{\mathrm{Ca}} \\ &\quad + k_c[\mathrm{Ca}])](v - V_{\mathrm{K}}) \\ &\quad + \bar{g}_{\mathrm{k}} \frac{\lambda}{\tau_n}(n_\infty - n)(v - V_{\mathrm{K}}), \\ H_2(v, n, [\mathrm{Ca}]) &= f_v(v, n, [\mathrm{Ca}]) \\ &= \bar{g}_{\mathrm{k}} n + \bar{g}_{\mathrm{sk}} s_\infty([\mathrm{Ca}]) \\ &\quad + \bar{g}_{\mathrm{bk}} \dot{f}_\infty(v)(v - V_{\mathrm{K}}) \\ &\quad + \bar{g}_{\mathrm{ca}} \dot{m}_\infty(v)(v - V_{\mathrm{K}}) + \bar{g}_{\mathrm{ca}} m_\infty(v) \\ &\quad + \bar{g}_{\mathrm{bk}} f_\infty(v), \end{aligned}$$

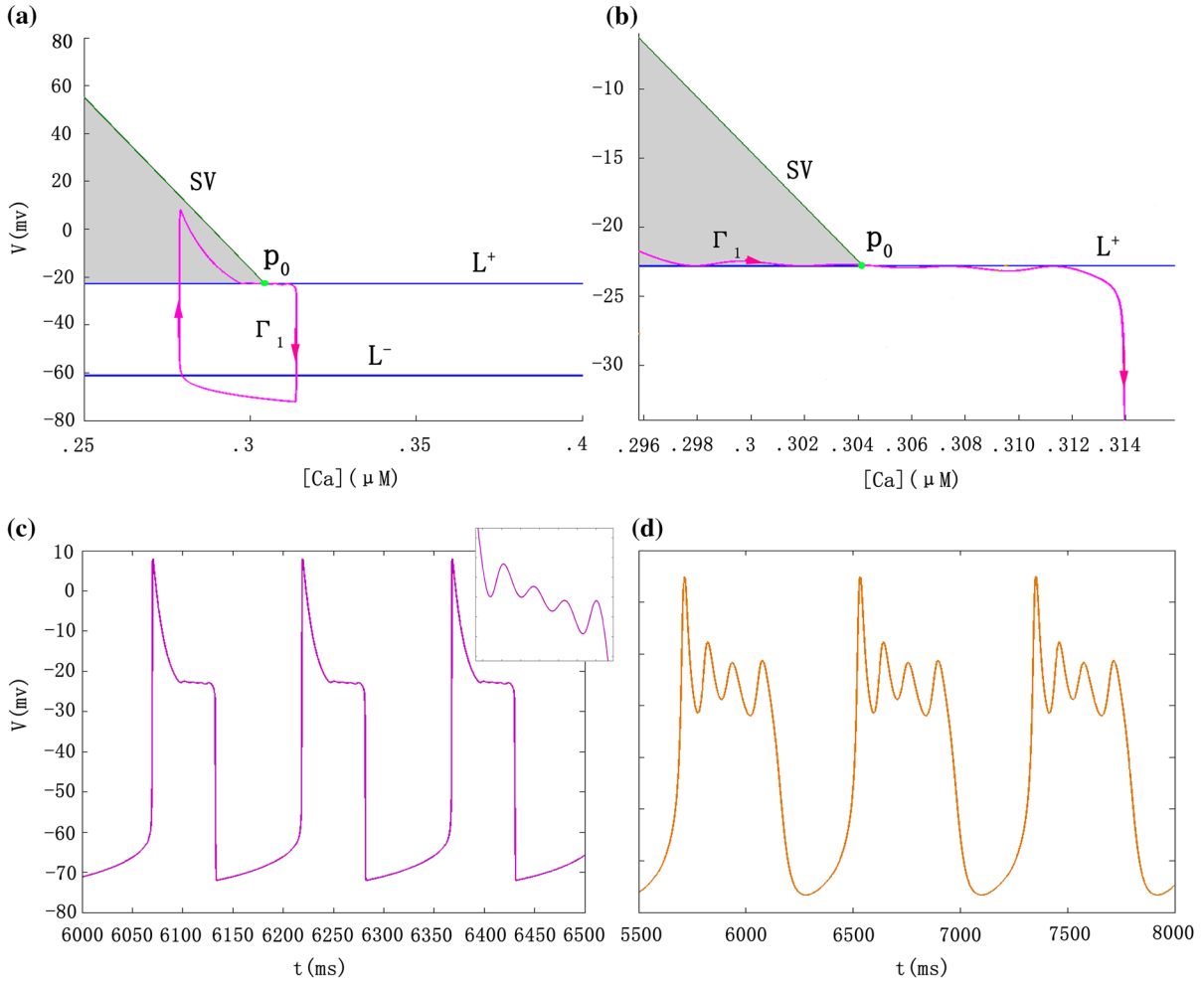

Fig. 2 The folded curve and the trajectories are projected to the $(V, [\mathrm{Ca}])$ plane. **a** Show the superimposed diagram; **b** the partial enlargement of **a**; **c**, **d** are the time series of membrane potential corresponding the trajectory of **a**

where "$\cdot$" indicates derivative with respect to time τ and A_0 denotes Jacobian matrix of the system.

Let λ_1, λ_2 denote the eigenvalues of Jacobian matrix A_0 at P_0, and it can be written as

$$A_0|_{P_0} = \begin{pmatrix} -9209836.318 & 466555.8231 \\ 0.00003163053013 & -0.0016 \end{pmatrix}.$$

Therefore, we can solve the eigenvalues $\lambda_1 = -9209836.318$, $\lambda_2 = -0.1598397647$, i.e., P_0 is a folded singular node. There exist singular canards, and it can always perturb to a maximal canard near the folded singular node. Readers can refer to [26–30] for a more detailed introduction to canards theory.

Statement 3 There exists a singular periodic orbit (pink line) $\Gamma = \Gamma_a \cup \Gamma_g$ for the system consists of Eqs. (5)–(7), the smooth segment Γ_a is the trajectory that is in the interior of the singular funnel with P_0 as the ending point, and $\Gamma_g = {\Gamma_a}^+ \cup {\Gamma_f}^+ \cup {\Gamma_a}^- \cup {\Gamma_f}^-$, where ${\Gamma_a}^\pm$ is the orbit to connect $L^\pm$ and $P(L^\mp)$, ${\Gamma_f}^\pm$ is the fast fibers to connect $L^\pm$ and $P(L^\pm)$. (Note: $P(L^\pm)$ is the trajectory, which is projected by $L^\pm$ along the direction of the fast fibers to the lower (upper) attracting branch of the critical manifold.)

As shown in Fig. 2, (a) the projection of two folded curve $L^\pm$ in the $(V, [\mathrm{Ca}])$ plane. The trajectory Γ_1 is the periodic orbits at $C_\mathrm{m} = 0.1$ pF. The curve $L^\pm$ is two folded curve, P_0 is the folded singular node, and SV denotes the strong eigendirection at the folded singular node. (b) is the partial enlargement of (a). (c) is time series of membrane potentials corresponding the phase

plane of (a). (d) is time sequences of membrane potentials at $C_{\mathrm{m}} = 15$ pF. Shadows of (a) are the singular funnel, and it is surrounded by the strong eigendirection SV and the folded curve L^{+}. There exist small amplitude oscillations in the funnel. Furthermore, we hope that there is a singular periodic orbit to connect the relaxation oscillations and the small amplitude oscillations. By theorem [30,37–39], we have an assumption that there exists a subset $N^{\pm} \subset P(L^{\mp})$ with the characteristic that it can arrive the folded curve $L^{\pm}$ when all trajectories of the slow subsystem satisfy the initial domains in $N^{\pm}$. So, the associated maps can be defined by $\prod^{\pm} : N^{\pm} \subset P(L^{\mp}) \mapsto L^{\pm}$. Moreover, the return map can be defined by $\prod \triangleq P \circ \prod^{+} \circ P \circ \prod^{-} : N^{-} \mapsto P(L^{+})$, and $\prod(N^{-}) \subset N^{-}$. According to the contracted mapping principle and Brouwer's fixed point theorem, we can prove the existence of singular periodic orbit. By the return map, small amplitude oscillations can return to the singular funnel, while mixed-mode oscillations emerge.

We can see that small amplitude oscillations can return the singular funnel by the map $\prod$. Therefore, MMOs emerge, and trajectory Γ_1 falls out of the singular funnel by the map $\prod$. So, we can obtain the above conclusion.

In this section, we use inherent initial values shown in Table 1 except that the membrane capacitance $C_{\mathrm{m}} = 0.1$ pF or $C_{\mathrm{m}} = 15$ pF. The reason for choosing them is that both sets of parameters can produce mixed-mode oscillations, but there is a set of trajectories that cannot fall into the singular funnel, which indicates that the theory is sufficient and not necessary. And we show that the MMOs of type 1^{s} appear by using the folded node theory, the error mainly comes from the accuracy of computer in the numerical procedure.

Therefore, we can obtain the following result.

Theorem 3.1 *Suppose that all assumptions in statement 1–3 are established, then for sufficiently small ε, there exists a stable MMO of type 1^{s} for the system consists of Eqs.* (5)–(7)*, for certainly determined $s > 0$.*

3.2 Two slow–two fast analysis of the whole system with four differential equations

By rescaling the time ($t = k_{t_1} t_1$), we introduce a dimensionless system that refers to the method of [33] as follows:

$$
\begin{aligned}
\varepsilon_1 \frac{\mathrm{d}V}{\mathrm{d}t_1} &= \frac{C_{\mathrm{m}}}{k_{t_1} g_{\mathrm{r}}} \frac{\mathrm{d}V}{\mathrm{d}t_1} \\
&= -\frac{1}{g_{\mathrm{r}}}(I_{\mathrm{Ca}} + I_{\mathrm{K}} + I_{\mathrm{SK}} + I_{\mathrm{BK}} + I_A) \\
&\triangleq f_1(V, h, n, [\mathrm{Ca}]), \\
\varepsilon_2 \frac{\mathrm{d}h}{\mathrm{d}t_1} &= \frac{\tau_h}{k_{t_1}} \frac{\mathrm{d}h}{\mathrm{d}t_1} = h_\infty - h \\
&\triangleq f_2(V, h), \\
\frac{\mathrm{d}n}{\mathrm{d}t_1} &= \frac{\lambda k_{t_1}}{\tau_n}(n_\infty - n) \\
&\triangleq h_1(V, n), \\
\frac{\mathrm{d}[\mathrm{Ca}]}{\mathrm{d}t_1} &= -k_{t_1} f_c k_c \left(\frac{\alpha}{k_c} I_{\mathrm{Ca}} + [\mathrm{Ca}] \right) \\
&\triangleq h_2(V, [\mathrm{Ca}]),
\end{aligned} \tag{8}
$$

where $k_{t_1} = \tau_n/\lambda$ is a scale factor, g_{r} is a reference conductance scale.

Here, we ignore the rescaling of V and [Ca] as they have no change in timescale. In our calculation, we implicitly assume that V is a non-dimensional variable and the result is stored in the dimensional form V. For system (8), we can know that the membrane voltage V is faster than other variables. As we can see that the gating variable n is slower than the activation variable h, while the calcium variable is essentially slower than other three variables. We introduce two small parameters $\varepsilon_1 = C_{\mathrm{m}}/(k_{t_1} g_{\mathrm{r}})$ and $\varepsilon_2 = \tau_h/k_{t_1}$, which will control the change of variables. By setting ε_1, we can better identify the timescale between V and $(h, n, [\mathrm{Ca}])$, while decreasing τ_h, the timescale of h and $(V, n, [\mathrm{Ca}])$ are separated. Here, we can obtain system (8) with two fast variables (V, h), two slow variables $(n, [\mathrm{Ca}])$ and two small parameters $(\varepsilon_1, \varepsilon_2)$. System (8) is described by two slow timescale; hence by converting the timescale $t_1 = \varepsilon_2 t_2$, we can obtain the fast timescale system (9):

$$
\begin{aligned}
\frac{\mathrm{d}V}{\mathrm{d}t_2} &= \frac{\varepsilon_2}{\varepsilon_1} f_1(V, h, n, [\mathrm{Ca}]), \\
\frac{\mathrm{d}h}{\mathrm{d}t_2} &= f_2(V, h), \\
\frac{\mathrm{d}n}{\mathrm{d}t_2} &= \varepsilon_2 h_1(V, n), \\
\frac{\mathrm{d}[\mathrm{Ca}]}{\mathrm{d}t_2} &= \varepsilon_2 h_2(V, [\mathrm{Ca}]).
\end{aligned} \tag{9}
$$

We are going to consider the change in two perturbation parameters. There are two situations, one is faster

than the other or both have the same timescale. Here, we assume that $\lim_{(\varepsilon_1,\varepsilon_2)\to(0,0)} \frac{\varepsilon_2}{\varepsilon_1} = r$, that is $\varepsilon_2 \to 0$ means that $\varepsilon_1 \to 0$. Therefore, letting $\varepsilon_2 \to 0$ (means $\varepsilon_1 \to 0$) in the fast system (9), we can obtain the 2D layer problem:

$$\begin{aligned}
\frac{\mathrm{d}V}{\mathrm{d}t_2} &= r f_1(V, h, n, [\mathrm{Ca}]),\\
\frac{\mathrm{d}h}{\mathrm{d}t_2} &= f_2(V, h),\\
\frac{\mathrm{d}n}{\mathrm{d}t_2} &= 0,\\
\frac{\mathrm{d}[\mathrm{Ca}]}{\mathrm{d}t_2} &= 0.
\end{aligned} \tag{10}$$

Similarly, letting $\varepsilon_2 \to 0$ in the slow timescale system (8), we can give the reduced problem:

$$\begin{aligned}
0 &= f_1(V, h, n, [\mathrm{Ca}]),\\
0 &= f_2(V, h),\\
\frac{\mathrm{d}n}{\mathrm{d}t_1} &= h_1(V, n),\\
\frac{\mathrm{d}[\mathrm{Ca}]}{\mathrm{d}t_1} &= h_2(V, [\mathrm{Ca}]).
\end{aligned} \tag{11}$$

By using the methods of asymptotic expansions, the analysis of the above two cases can characterize the solution of the original system to a certain extent. Our purpose is to understand the original 4D system based on the 2D layer problem and 2D reduced problem using GSPT. We exhibit only a cursory analysis whilst emphasizing the MMOs is produced by canard phenomenon.

First, we have to do an analysis of 2D layer problem. The nature of layer problem is to consider slow variable as a parameter in system (10). Next, we give the equilibria of the layer problem, that is called critical manifold. $SS = \{V, h, n, [\mathrm{Ca}]) \in R^4,\ f_1(V, h, n, [\mathrm{Ca}]) = f_2(V, h) = 0\}$. Obviously, we can see that it is a folded surface and the fold bifurcation curve can be denoted as $L = \{(V, h, n, [\mathrm{Ca}]) \in SS,\ \det(J_r) = f_{1V} f_{2h} - f_{1h} f_{2V} = 0\}$, where $J_r = \begin{pmatrix} f_{1V} & f_{1h} \\ f_{2V} & f_{2h} \end{pmatrix}$.

The attraction sheets SS_a (in SS) and repelling sheets SS_r (in SS) are separated by two folded curves. All trajectories of the initial condition that are not on the critical manifold will eventually be confined to the critical manifold. Once the trajectory enters the critical manifold, the layer problem may be out of operation on it and slow variable will contribute the major domination. Therefore, we will use the slow equation to analyze dynamics via the reduced problem.

By considering the layer problem, we can give the projection system of reduced problem as:

$$\begin{aligned}
(\det J)\frac{\mathrm{d}V}{\mathrm{d}t_1} &= -f_2 h(f_{1n} h_1 + f_{1[\mathrm{Ca}]} h_2),\\
\frac{\mathrm{d}[\mathrm{Ca}]}{\mathrm{d}t_1} &= h_2(V, [\mathrm{Ca}]).
\end{aligned} \tag{12}$$

We can obtain the desingularized system by time rescaling ($t_1 = det(J)\tau_1$) to eliminate the singular term.

$$\begin{aligned}
\frac{\mathrm{d}V}{\mathrm{d}\tau_1} &= -f_2 h(f_{1n} h_1 + f_{1[\mathrm{Ca}]} h_2) \triangleq F,\\
\frac{\mathrm{d}[Ca]}{\mathrm{d}\tau_1} &= \det(J) h_2.
\end{aligned} \tag{13}$$

Therefore, we can see that there are two kinds of singularities: one is ordinary singularity, which consists of the equilibria of the reduced problem and the other is folded singularity, which can be given by $L_0 = \{(V, n, h, [\mathrm{Ca}]) \in L,\ F = 0\}$. In these folded singularities, both sides of the V-equation of system (12) are equal to zero simultaneously. That means dV/dt is finite at folded singularity. This means that the trajectory will take turns through the fold L within a controllable time. These solutions are called singular canards, and it will exist until small perturbations vary greatly in complex dynamics.

We can combine analysis of layer problem with exploration of reduced problem to understand dynamical behaviors of the 4D system. We describe the formation of periodic solutions. The trajectory begin from the fold L^- along the fast fibers to the upper attracting branch; then, the flow is controlled by system (11) until it reaches fold L^+. Therefore, the layer problem illustrates transition of down-jump (up-jump) and the reduced problem explains the process of trajectory on the critical manifold. Therefore, there exists a relaxation oscillation, which is similar to Sect. 3.1, and it corresponds to the spiking of system consists of Eqs. (1)–(4).

We exhibit graphic rendering of the critical manifold in Fig. 3. The critical manifold can be shown in the three-dimensional phase space, and the resulting mixed-mode oscillation is very sensitive to changes in membrane capacitance. The initial values are shown in Fig. 3.

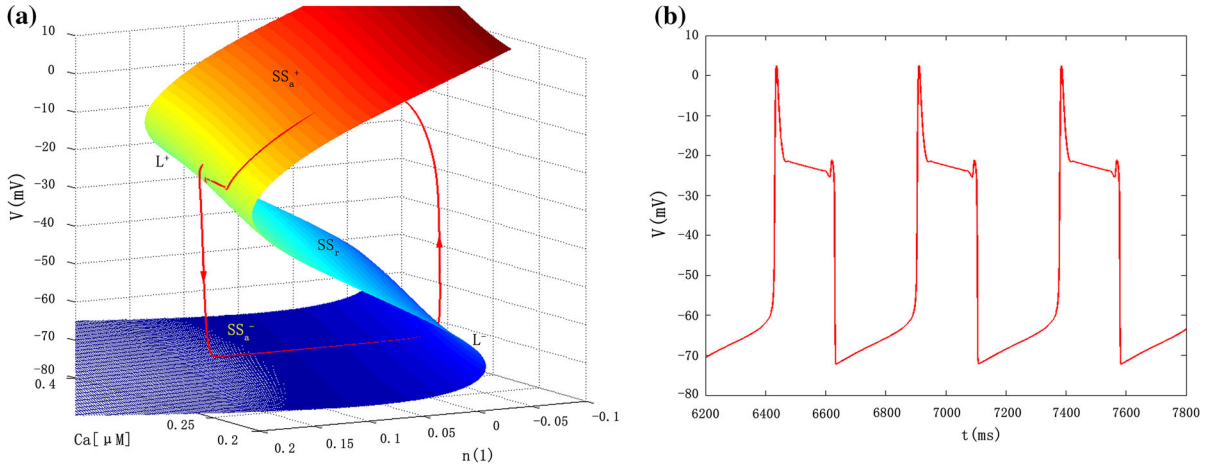

Fig. 3 4D system with the MMOs. **a** Singular orbit and critical manifold are composed of the projection of system (10) and (11) on the (V, n, [Ca]) space; **b** mixed-mode oscillations correspond to the trajectory of **a**. Modified parameters: $C_{\mathrm{m}} = 0.5$ pF, $\tau_h = 2.0$ ms, $g_a = 18$ nS and other parameters are given in Table 1

3.3 One slow–three fast dynamics illustration of the whole system

There may be two origins for the generation of bursting of the pituitary lactotroph model. One is the opening of Ca^+ channels [2], and the other is that A-type K^+ current can trigger the generation of bursting [4]. The existence of mixed-mode oscillations is illustrated in the preamble. In this section, we will use the slow–fast dynamics to demonstrate the transition between firing state and quiescent state. The corresponding diagram is provided in Fig. 4.

Some researchers use average voltage to study the fast–slow system [13]. We will investigate whether it is possible to determine the transition mechanism via one slow–three fast dynamics analysis. Teka and his collaborators have already made the transition from plateau to pseudo-plateau bursting via transforming the parameters (v_n, v_{m}, g_{k} et al.) and vice versa [40]. That means, it requires us to analyze superimposed bifurcation diagram. In the following, we give a cursory analysis of the three superimposed cases. In Fig. 4a, left-hand shows the bifurcation diagram of fast subsystem with slow variable [Ca] as a bifurcation parameter and the [Ca]-nullcline is superimposed the bifurcation diagram. There is no stable limit cycle of the fast subsystem, and it has a periodic spiking, which is aroused from the saddle-node LP_1. In Fig. 4, all parameters are set to $C_{\mathrm{m}} = 10$ pF, g_{bk} is varied, and others are frozen in Table 1.

In Fig. 4b, an unstable limit cycle emerges via the subcritical Hopf bifurcation point and a stable limit cycle appears by the saddle-node cycle bifurcation. At that moment, they are coexisting and pseudo-plateau bursting occurs. The fast subsystem is bistable in a small range of [Ca] value, and it contains the depolarized upper steady state consists of the stable limit cycle and hyperpolarized lower steady state consists of the stable node. The electrical activity is depolarized in the saddle-node point LP_2, but finally we cannot use the normal bursting classification to analyze how it is to reach the quiescent steady state, although it is like the "fold/homoclinic" bursting mode. This may depend on the difference between fast timescale and slow timescale, and the emergence of PD may be also one of the important reasons.

The subcritical Hopf bifurcation will move to the right when g_{bk} is decreased to -2.0 nS. There is no stable periodic spiking in the fast subsystem, and the unstable limit cycle exists in the small range of [Ca] value as shown in Fig. 4c. Bistability occurs in a tiny range while accompanying by the rapid change of periodic spiking, and the [Ca] concentration is quickly gathered or subsided. The bifurcation diagram may be considered as "fold/Hopf" bursting mode if not to consider the situation of the limit cycle. The pattern is produced by saddle-node LP, and finally, the oscillation

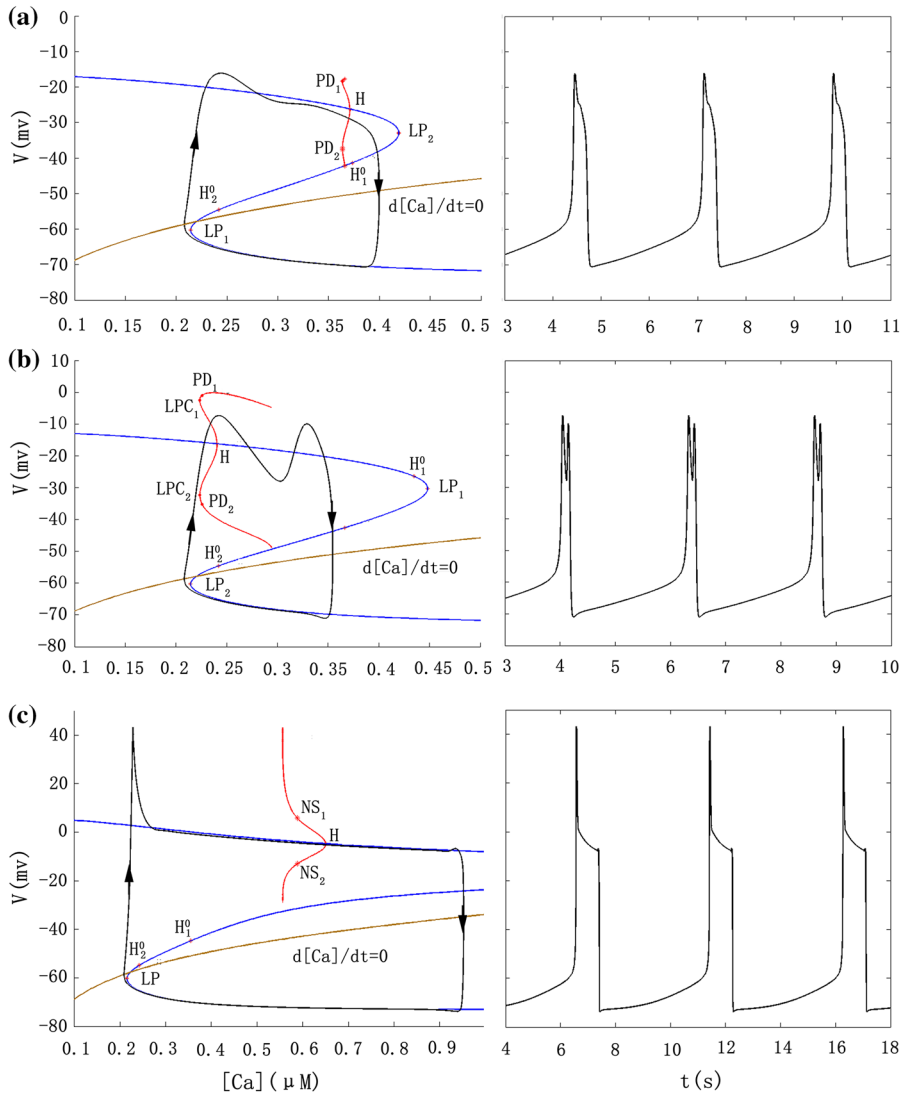

Fig. 4 Slow–fast dynamics analysis for $C_{\mathrm{m}} = 10pF$, and different conductance values for g_{bk}. The blue "z-curve" is equilibria curve of fast subsystem. The red line represents the maximum and minimum value of limit cycles, the black closed line of left panel is (V, n) phase plane, and the right indicates the corresponding membrane voltage sequence diagram. All labels are as follows: LP_i represents the saddle-node bifurcation point, PD_i represents the flip bifurcation, H denotes the Hopf bifurcation point, ${H^0}_i$ indicates the neutral saddle, LPC denotes fold cycle bifurcation, and NS_i represents the Neimark–Sacker bifurcation. **a** $g_{\mathrm{bk}} = 0.5$ nS, the whole system can produce periodic spiking, and its appearance just has little relationship to the bifurcation of fast subsystem; **b** $g_{\mathrm{bk}} = 0$ nS, pseudo-plateau bursting oscillation occurs. The stable and unstable limit cycles are coexisting, and the model exhibits the bistable steady state in the tiny range of [Ca] value. **c** $g_{\mathrm{bk}} = -2.0$ nS, signature 1^s mixed-mode oscillation emerges, which is similar to "fold/Hopf" discharge mode. (Color figure online)

decays to steady resting state via the unstable Hopf bifurcation. NS bifurcation and other kinetic parameters may have an impact on it.

The result illustrates the idea that which method we should use to solve the question depends on the difference between fast variable and slow variable. In most cases, bursting transition mechanism is explored to use one slow variables dynamics analysis, and bursting pattern can be well categorized. But if the slow variable is not obvious enough, the two slow variables will be

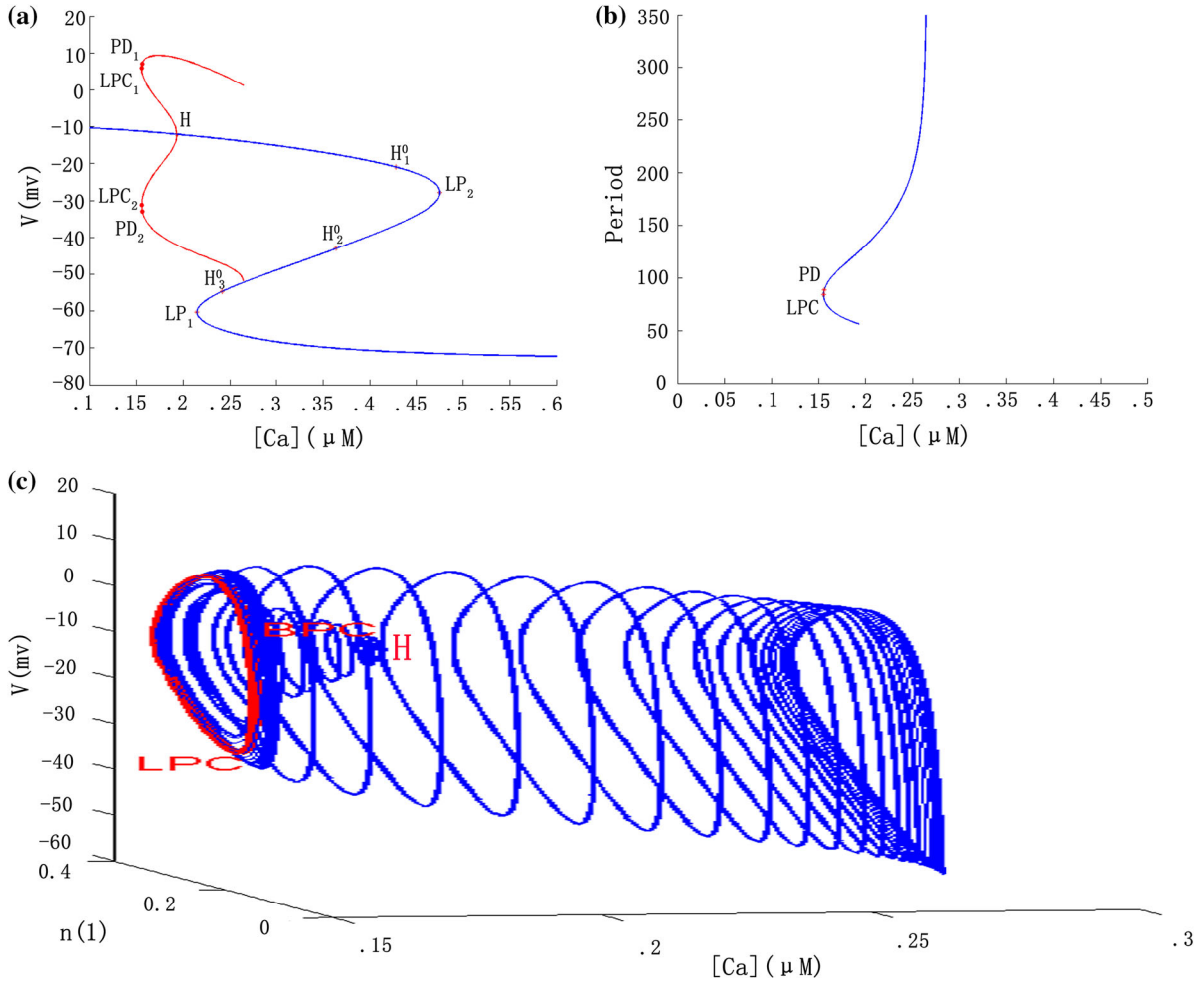

Fig. 5 Bifurcation diagram of [Ca] as the bifurcation parameter. **a** Equilibria of the fast subsystem, the lower branch of "z-curve" is occupied by the node, the middle and the upper are saddle, the red line represents the maximum and minimum values of limit cycle. **b** Period transition of limit cycles. **c** The spatial map of limit cycle in $(v, n, [\mathrm{Ca}])$ phase plane. The corresponding labels are as follows: LPC_i represents the saddle-node of limit cycle, PD_i represents the flip bifurcation, H denotes the Hopf bifurcation point , $H^0{}_i$ indicates the neutral saddle, LP_i represents the saddle-node bifurcation point, BPC represents the branch point of cycle. (Color figure online)

a more meaningful way to analyze the system from another level. Certainly, we are required to determine the one-dimensional fast subsystem via decreasing the membrane capacitance C_{m}. That is to say, with the decrease in membrane capacitance, the analysis of one fast variable may be better. In summary, we will focus on the classification of subsystems for better use of slow–fast dynamics.

4 Codimension-one bifurcation analysis

As the same as Sect. 3.3, we use the slow variable as a bifurcation parameter. As shown in Fig. 5a, we will determine stability of the Hopf bifurcation point via calculating the first Lyapunov coefficient. We all know Hopf bifurcation is supercritical (or subcritical) if the first Lyapunov coefficient is negative (or positive). Here, we adopt the bifurcation diagram when $g_{\mathrm{bk}} = 0.3$ nS and other parameters are given in Table 1. Some numerical results are explained later. Following

this idea, we have a detailed calculation in "Appendix A."

The first Lyapunov coefficient is a index of stability of the equilibrium, which is produced when the two-dimensional system is transformed into a poincare normality at the Hopf equilibrium. For high-dimensional systems, we need to calculate the norms in the center manifold. From the above, we can obtain the first Lyapunov coefficient via applying the invariant expression (5.62) in [41].

$$\begin{aligned} l_1(0) = \frac{1}{2\omega_0}\mathrm{Re}\Big\{ & \langle p, C(q,q,\overline{q})\rangle \\ & -2\Big\langle p, B(q, A^{-1}B(q,\overline{q}))\Big\rangle \\ & +\Big\langle p, B(\overline{q}, (2i\omega_0 E - A)^{-1}B(q,q))\Big\rangle\Big\} \\ = & \ 0.0042112 > 0. \end{aligned}$$

Hence, H is a subcritical Hopf bifurcation point and it can branch out the unstable limit cycle.

From above, we can know that it produces an unstable limit cycle starting from the Hopf bifurcation point H. Moreover, we can find that the period of limit cycle is increased with the decrease in [Ca] value as shown in Fig. 5a, b. Stable and unstable limit cycle coexists in the fast subsystem via the limit point of cycle and a flip bifurcation occurs. Limit cycle will always exist until a stable limit cycle hits the saddle point in the middle branch of the bifurcation curve to form a saddle homoclinic bifurcation. Meanwhile, the period of limit cycle varies greatly. And ultimately, it breaks through a bounded value to infinity when the [Ca] value is a determined constant between 0.25 and 0.3 μM, which may be able to form a homoclinic orbit. Furthermore, branching point cycle is detected when we take the PD bifurcation point as starting point to explore the limit cycle, and that is clearer to observe the transition process of the limit cycle by exhibiting it in Fig. 5c.

5 Codimension-two bifurcation analysis

In this section, we will analyze the whole system that consists of Eqs. (1)–(4), and we focus on analyzing its cusp bifurcation, Bautin bifurcation and Bogdanov–Takens bifurcation. Its initial values are given in Table 1. Singular point coordinates can vary greatly even when there are small perturbations in this set of parameters. We use the MAPLE software that is a symbolic package for calculation and analysis.

5.1 Analysis in the (g_{bk}, g_{sk}) phase plane

As shown in Fig. 6, we demonstrate two-parameter bifurcation plane of the whole system via numerical simulation, and related kinetic parameters are given in Table 1. (a) Exhibiting the codimension-two bifurcation diagram. (b), (c) are the partial enlargement of bifurcation diagram (a). (d) Exhibiting the PD bifurcation curve that is found starting from the PD point. In Fig. 6, the meaning of each label is explained as follows: GH_i $(i = 1, 2, 3, 4, 5)$ represents the Bautin bifurcation; CP_i $(i = 1, 2, 3)$ represents the cusp bifurcation; ZH represents the fold-Hopf bifurcation; BT represents the Bogdanov–Takens bifurcation; $LPNS$ represents fold-Neimark–Sacker bifurcation; $R1$ represents 1:1 resonance; $R2$ represents 1:2 resonance; $LPPD$ represents the fold-flip bifurcation. Readers can refer to [41,42] for a detailed illustration of all the bifurcation labels. Some of the data at these special bifurcation point are shown in Table 2.

From Fig. 6a, we can know that the change in saddle-node bifurcation curve f_1 is independent on the conductance g_{sk} and there is no codimension-two bifurcation point on it. There is a little information in the Hopf curve h_2. Most of codimension-two bifurcation points are situated on the saddle-node curve f_2 and the Hopf curve h_1. There is a LPC curve between the $R1_1$ and the $R1_2$, and it coincides with the part of the Hopf bifurcation curve h_1, although that is not easy to identify. CP_1 is a termination point of saddle-node bifurcation curve f_1 and f_2. Saddle-node bifurcation curve f_2 is divided into three sections by marking the cusp point CP_2 and CP_3.

Near the cusp point CP_1 $(-3.665138, 1.171912)$, the system's eigenvalues are $\lambda_1 = 0, \lambda_2 = -0.239172$, $\lambda_3 = -0.049999$, $\lambda_4 = -0.0290647$. The differential system is locally topologically equivalent to following normal forms:

$$\begin{cases} \dot{\eta} = \beta_1 + \beta_2\eta + s\eta^3, & \eta \in R^1, \\ \dot{\xi}_- = -\xi_-, & \xi_- \in R^3, \end{cases}$$

where $\beta_1, \beta_2 \in R$, $s = \mathrm{sign}(c) = -1$.

Near the cusp point CP_2 $(-14.741551, 18.745219)$, the system's eigenvalues are $\lambda_1 = 0$, $\lambda_2 = -0.0500106$, $\lambda_3 = 0.0283496$, $\lambda_4 = 0.273392$, and CP_3 $(-2.264354, 3.503469)$, the system's eigenvalues are $\lambda_1 = 0$, $\lambda_2 = -0.0502939$, $\lambda_3 = -0.011844$, $\lambda_4 = 0.54639$. The differential system is locally topologically equivalent to following normal forms:

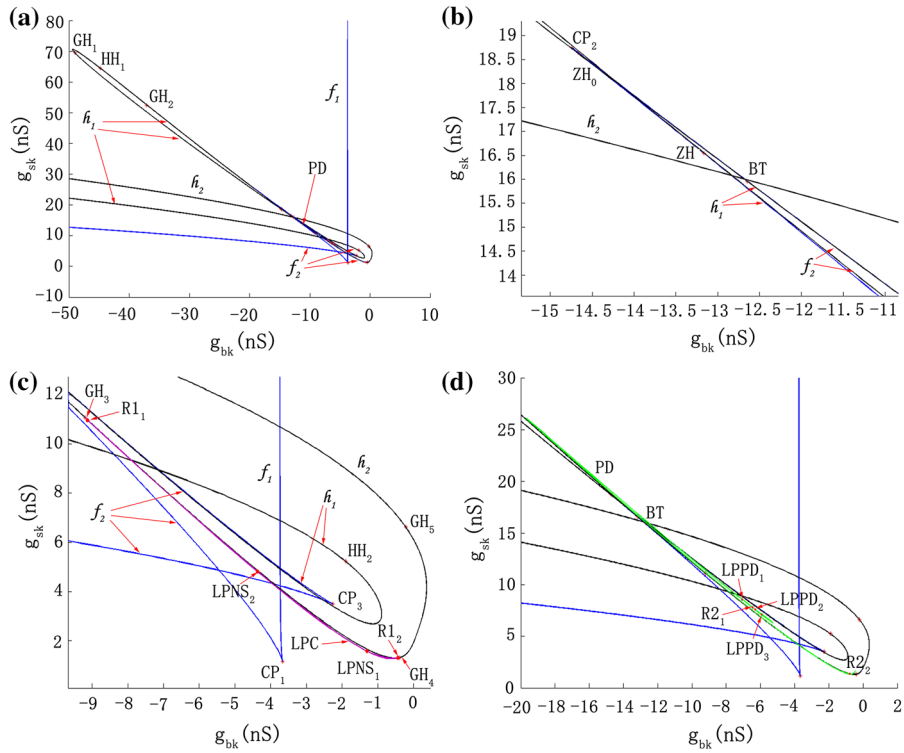

Fig. 6 Codimension-two bifurcation diagram of the whole system. **a** Two-parameter bifurcation on the (g_{bk}, g_{sk}) phase plane. **b**–**d** are partial enlargement of the bifurcation diagram **a**. The corresponding labels are as follows: f_1 and f_2 are the saddle-node bifurcation curves, h_1 and h_2 are the Hopf bifurcation curves, GH_i-generalized Hopf (Bautin), HH_i-neutral saddle, PD-flip bifurcation curve (green line), LPC-fold cycle bifurcation curve (pink line), ZH_0-zero-neutral saddle, ZH-fold-Hopf, CP_i-cusp, BT-Bogdanov–Takens, $R1_i$-1:1 resonance, $LPNS_i$-fold-Neimark–Sacker, $R2_i$-1:2 resonance and $LPPD_i$-fold-flip. (Color figure online)

$$\begin{cases} \dot{\eta} &= \beta_1 + \beta_2\eta + s\eta^3, \quad \eta \in R^1, \\ \dot{\xi}_- &= -\xi_-, \\ \dot{\xi}_+ &= \xi_+, \end{cases}$$

where $\beta_1, \beta_2 \in R$, $s = \text{sign}(c) = 1$, $\xi_- \in R^1$, $\xi_+ \in R^2$ for CP_2, $\xi_+ \in R^1$, $\xi_- \in R^2$ for CP_3.

In Table 2, we can see that there are five Bautin bifurcation points on two bifurcation curves. There are a pair of pure imaginary eigenvalues and two nonzero real eigenvalues, and the first Lyapunov coefficient is equal to zero at these Bautin bifurcation points. Near the Bautin bifurcation point GH_j $(j = 1, 2)$, the differential system is locally topologically equivalent to following normal forms:

$$\begin{cases} \dot{z} &= (\beta_1 + i)z + \beta_2 z|z|^2 + sz|z|^4, \quad z \in C^1, \\ \dot{\xi}_- &= -\xi_-, \quad \xi_- \in R^1, \\ \dot{\xi}_+ &= \xi_+, \quad \xi_+ \in R^1, \end{cases}$$

where $\beta_1, \beta_2 \in R$, $s = \text{sign}(l_2) = -1$.

Near the bifurcation point GH_j $(j = 3, 4, 5)$, the differential system is locally topologically equivalent to following normal forms:

$$\begin{cases} \dot{z} &= (\beta_1 + i)z + \beta_2 z|z|^2 + sz|z|^4, \quad z \in C^1, \\ \dot{\xi}_- &= -\xi_-, \quad \xi_- \in R^2, \end{cases}$$

where $\beta_1, \beta_2 \in R$, $s = \text{sign}(l_2) = -1$.

Specially, the Hopf bifurcation curve h_1 is tangent to the saddle-node bifurcation curve f_2 at codimension-two Bogdanov–Takens bifurcation. It has two zero eigenvalues $\lambda_{1,2} = 0$ and two nonzero real eigenvalues $\lambda_3 = -0.0500154$, $\lambda_4 = 0.635512$. Near the Bogdanov–Takens bifurcation point, the differential system is locally topologically equivalent to following normal forms:

$$\begin{cases} \dot{\eta}_1 &= \eta_2, \\ \dot{\eta}_2 &= \beta_1 + \beta_2\eta_1 + {\eta_1}^2 + s\eta_1\eta_2, \\ \dot{\varsigma}_- &= -\varsigma_-, \quad \varsigma_- \in R^1, \\ \dot{\varsigma}_+ &= \varsigma_+, \quad \varsigma_+ \in R^1, \end{cases}$$

where $\beta_1, \beta_2 \in R$, $s = \text{sign}(ab) = 1$, $(\eta_1, \eta_2)^{\text{T}} \in R^2$.

Furthermore, there is a fold-Hopf bifurcation point, which is labeled ZH with one zero eigenvalue, a pair of pure imaginary eigenvalues and one nonzero real eigenvalue, but there is no fixed normal form in the case $(s = 1, \theta = -1.710129 \times 10^2)$. There exist three neutral saddles, which are labeled ZH0 (zero-neutral saddle, one zero eigenvalue and two real eigenvalues that satisfy their sum is equal to zero), HH_1 (Hopf-neutral saddle, a pair of pure imaginary eigenvalues and two real eigenvalues that satisfy their sum is equal

to zero) and HH_2 (two pairs of real eigenvalues satisfy the sum of each pair is equal to zero), respectively.

5.2 Bogdanov–Takens bifurcation

In this section, we investigate the Bogdanov–Takens bifurcation by the theoretical method that is implemented in [43]. In the whole system, we use (g_{bk}, g_{sk}) as a pair of bifurcation parameter, and other parameters are shown in Table 1. In Fig. 6a, the Bogdanov–Takens bifurcation point emerges when $(g_{bk}, g_{sk}) = (-12.645060, 15.956172) \triangleq \mu_0$ and its coordinate is $(V, n, h, [Ca]) = (-4.071616, 0.523193, 0.000014, 0.801346) \triangleq X_0$. The detailed proof process is in "Appendix B."

From the preceding analysis, we can obtain the following main results by using the method in [41].

Theorem 5.1 *Let (X_0, μ_0) be a Bogdanov–Takens bifurcation point of the whole system that consists of Eqs. (1)–(4). Note that $\lambda_1 = g_{bk} + 12.645060$, $\lambda_2 = g_{sk} - 15.956173$, if $0 < \| (\lambda_1, \lambda_2) \|^2 \ll 1$, the dynamics on the center manifold of the system near $X = X_0$, $\mu \approx \mu_0$ is locally topologically equivalent to the following system*

$$\begin{aligned}
\frac{d\eta_1}{dt_1} &= \eta_2,\\
\frac{d\eta_2}{dt_1} &= 4.05839597 \times 10^4\lambda_1 + 3.091079973 \times 10^4\lambda_2\\
&\quad + \left(-36.06012167\lambda_1 - 5.537943388 \times 10^7\lambda_2\right)\eta_1\\
&\quad + {\eta_1}^2 + \eta_1\eta_2,
\end{aligned}$$

which have three local representation of bifurcation curves in the small neighborhood near the origin:

(i) there exists a saddle-node bifurcation curve

$$\begin{aligned}
SN = \{(\lambda_1, \lambda_2) :\ & 0.008010137408{\lambda_1}^2\\
& + 2.460318237 \times 10^4\lambda_1\lambda_2\\
& + 1.889220347 \times 10^{10}{\lambda_2}^2\\
& - \lambda_1 - 0.7616506608\lambda_2 = 0\};
\end{aligned}$$

(ii) there exists a Hopf bifurcation curve

$$H = \{(\lambda_1, \lambda_2) :\ \lambda_1 + 0.7616506608\lambda_2 = 0,\ \lambda_2 < 0\};$$

(iii) there exists a saddle homoclinic bifurcation curve

$$\begin{aligned}
Hom = \{(\lambda_1, \lambda_2) :\ & 0.007689731910{\lambda_1}^2\\
& + 2.361905508 \times 10^4\lambda_1\lambda_2\\
& + 1.813651533 \times 10^{10}{\lambda_2}^2\\
& + \lambda_1 + 0.7616506608\lambda_2\\
= o & \left(\|(\lambda_1, \lambda_2)\|^2\right),\\
& \lambda_1 + 1.535752829 \times 10^6\lambda_2 < 0\}.
\end{aligned}$$

6 Discussion

The transition has been explored from tonic spiking to bursting when only BK-type potassium channel or A-type potassium channel is added to the original system. There are different mathematical mechanisms even though they are both influencing the increase or decrease in calcium concentration. The model we have considered is simultaneously adding both BK-type channels and A-type channels to the original pituitary model. We mainly explored the mathematical mechanism of mixed-mode oscillations via using geometric singular perturbation theory, and we theoretically calculated the dynamical properties near the Bogdanov–Takens bifurcation by using the bifurcation theory and the center manifold theorems. Its dynamical behavior is different from merely adding a fast potassium ion channel to the system, and it may have an adequate guide to model improvement.

The pituitary lactotroph can promote development of the mammary gland which plays a vital role in stimulating and maintaining prolactin levels. Bursting and tonic spiking are effective translation for signals between neurons. Therefore, it is essential that we explore electrical activity of the lactotroph model to understand physiological meaning in the real neural networks with large number of neurons. In this study, we have researched the dynamical mechanism that is hidden in the bursting electrical activity via using two different timescale analysis. And we also have drawn a comparison between different timescale. Based on these results, we propose that which one we should use will be more effective depending on the appropriate conditions. Moreover, we also have demonstrated behavior of bifurcation point by multi-parameter bifurcation analysis in a small range.

In this paper, mixed-mode oscillation has been discovered and we have proved the existence of signa-

ture 1^s by using geometric singular perturbation theory, which is greatly an effective way to analyze the dynamics of a system. In particular, we have showed the generation mechanism of MMOs by using the folded node singular theory. We found a fly in the ointment: it is not to estimate the number of small amplitude oscillations. Because relevant theory of MMOs is incomplete for nonlinear system, and it shows only folded node singular theory and singular Hopf theory to explain the existence of MMOs. These two conditions are sufficient but not necessary. We have privately calculated the MMOs as shown in Fig. 2d, but it is not satisfied with the above two theories (no show). Therefore, these are still very mysterious to us for further research and they also become our focus. Furthermore, the dynamical patterns of electrical activity were explained by using slow–fast dynamics analysis, which has been used frequently in the classification of bursting pattern and it had a great development in the later. We have used this method to illustrate many bursting modes and discharge types. A variety of bursting patterns appeared in our model with pseudo-plateau bursting, and we explained the firing mechanism to a certain extent. From the above discussion, we can see that it is necessary to identify fast kinetic variable and slow kinetic variable. In addition, we calculated the first Lyapunov coefficient of Hopf bifurcation to determine whether it forms a stable limit cycle, and in our calculations, the first Lyapunov coefficient is positive; hence, it has to generate an unstable limit cycle via the Hopf bifurcation. The transition of electrical activity was illustrated by describing the stability of limit cycle. Particularly, stable limit cycle corresponds to the tonic spiking and unstable limit cycles are associated with the transition of tonic spiking to bursting. Finally, we mainly discussed the property of Bogdanov–Takens bifurcation by two-parameter bifurcation analysis. We not only calculated the local topologically equivalent normal forms but also theoretically determined the existence of three bifurcation curves near the Bogdanov–Takens bifurcation. Trajectories of these bifurcation curves are not easily found in drawing them by MATCONT when saddle-node bifurcation curve and Hopf bifurcation are very close. These results have a positive effect on us to better understand bursting pattern of discharge activity.

7 Conclusions

Compared with the mixed-mode oscillation of the three-dimensional system appearing in previous publications, the paper is mainly manifested in demonstrating concrete implementation steps of the existence of mixed-mode oscillations and we combine theory and graphics to suggest that fold node singular theory guarantees its existence for the three-system with only a BK-type potassium channel. Furthermore, it is illustrated that this condition is sufficient but not necessary. (As shown in Fig. 2d, fold node theory cannot guarantee its existence even though it presents mixed-mode oscillations.) These are different from the sketch interpretation of mixed-mode oscillation in the published literature.

Real biological neurons actually have A-type potassium channels (fast, inactivating) and BK-type potassium channels (fast, activating), which have a defined expression of ion currents. Further three-dimensional and four-dimensional system have different dynamic behaviors. By comparing the analysis of three-dimensional and four-dimensional models, we find that the number of singular points does not change, but their coordinate is significantly different. But analysis of three-dimensional model is relatively explicit, there is less discussion of four-dimensional model. Therefore, we divide the system into one slow–three fast or two fast–two slow subsystem to propose that which one we should select will be more effective method to analyze a differential system depending on the timescale of subsystem and perform codimension analysis to the four-dimensional system. Equivalent form and three local representations of bifurcation curves have been investigated. The above results have deepened our understanding of dynamics of neuron discharge, and discharge behavior is closely associated with neurological information.

Acknowledgements The author acknowledges the referees and the editor for carefully reading this paper and suggesting many helpful comments. Thanks for all author contributions: F. Zhan contributed to the numerical and theoretical analysis, graphic processing and wrote the manuscript. S. Liu contributed to the structure and design of the study, and revised the manuscript. B. Lu provides part of the writing instruction. X. Zhang and J. Wang contributed to polish the English expression and final presentation of the paper. This work was supported by

the National Natural Science Foundation of China under Grant Nos. 11172103 and 11572127.

Compliance with ethical standards

Conflict of interest The authors declare that the research was conducted in the absence of any commercial or financial relationships that could be construed as a potential conflict of interest.

Appendix A

We rewrite the fast subsystem of the whole system as:

$$\begin{aligned}\frac{\mathrm{d}V}{\mathrm{d}t} &= F_1(V,n,h,[\mathrm{Ca}]),\\ \frac{\mathrm{d}n}{\mathrm{d}t} &= F_2(V,n),\\ \frac{\mathrm{d}h}{\mathrm{d}t} &= F_3(V,h),\end{aligned} \tag{14}$$

where

$$\begin{aligned}F_1 &= -\frac{1}{C_\mathrm{m}}F_0,\\ F_2 &= \frac{\lambda}{\tau_n}(n_\infty(V)-n),\\ F_3 &= \frac{1}{\tau_h}(h_\infty(V)-h),\\ F_0 &= g_{\mathrm{ca}}m_\infty(V)(V-V_{\mathrm{Ca}}) + g_{\mathrm{k}}n(V-V_{\mathrm{K}})\\ &\quad + g_{\mathrm{sk}}s_\infty([\mathrm{Ca}])(V-V_{\mathrm{K}}) + g_{\mathrm{bk}}f_\infty(V)(V-V_{\mathrm{K}})\\ &\quad + g_a a_\infty(V)h(V-V_{\mathrm{K}}),\end{aligned}$$

where $m_\infty(V)$, $s_\infty([\mathrm{Ca}])$, $f_\infty(V)$, $a_\infty(V)$ and related parameters are defined in Sect. 2.

The Jacobian matrix A of the fast subsystem (14) can be written as:

$$A = \begin{pmatrix} \frac{\partial F_1}{\partial V} & \frac{\partial F_1}{\partial n} & \frac{\partial F_1}{\partial h} \\ \frac{\partial F_2}{\partial V} & \frac{\partial F_2}{\partial n} & \frac{\partial F_2}{\partial h} \\ \frac{\partial F_3}{\partial V} & \frac{\partial F_3}{\partial n} & \frac{\partial F_3}{\partial h} \end{pmatrix}.$$

The fast subsystem has an equilibria H when we take $[\mathrm{Ca}] = 0.193055$, the Jacobian matrix A at H can be represented as:

$$A = \begin{pmatrix} 0.02319841247 & -25.16964160 & -108.2843060 \\ 0.0005160044168 & 0.02333333333 & 0 \\ 0.0000006875519 & 0 & -0.05 \end{pmatrix}$$

with a pair of conjugate pure imaginary roots λ, $\bar{\lambda}$, and $\lambda = iw$, $w = 0.111259$, another eigenvalue $\lambda_1 = -0.0501334$. There is a Hopf bifurcation in the fast subsystem as shown in Fig. 5a. $q = (0.999989698, 0.000931642 - 0.0044424375i, -0.0000023105 + 0.0000051416i)^{\mathrm{T}}$ is an eigenvector of λ, which satisfies $Aq = \lambda q$, $A\bar{q} = \bar{\lambda}\bar{q}$ and the adjoint eigenvector p satisfies $A^{\mathrm{T}}p = \bar{\lambda}p$, $A^{\mathrm{T}}\bar{p} = \lambda\bar{p}$ and normalization $\langle p, q\rangle = 1$, here $\langle p, q\rangle = \bar{p}_1q_1 + \bar{p}_2q_2 + \bar{p}_3q_3$ is the standard scalar product in C^3. Therefore, we take p as $(0.499885101 + 0.104312573i, -0.112746356 - 113.063114i, -97.4196870 - 442.649734i)^{\mathrm{T}}$.

We transform the equilibria H to coordinate origin to calculate the first Lyapunov coefficient. Next, we will make the following transformation:

$$\begin{cases} V = \xi_1 + V_0, \\ n = \xi_2 + n_0, \\ h = \xi_3 + h_0, \end{cases}$$

The fast subsystem (14) can be converted to the following:

$$\begin{aligned}\frac{\mathrm{d}V}{\mathrm{d}t} &= -\frac{1}{C_\mathrm{m}}G,\\ \frac{\mathrm{d}n}{\mathrm{d}t} &= \frac{\lambda}{\tau_n}(n_\infty(\xi_1+V_0)-\xi_2-n_0),\\ \frac{\mathrm{d}h}{\mathrm{d}t} &= \frac{1}{\tau_h}(h_\infty(\xi_1+V_0)-\xi_3-h_0),\end{aligned} \tag{15}$$

where

$$\begin{aligned}G &= g_{\mathrm{ca}}m_\infty(\xi_1+V_0)(\xi_1+V_0-V_{\mathrm{Ca}})\\ &\quad + g_{\mathrm{k}}(\xi_2+n_0)(\xi_1+V_0-V_{\mathrm{K}})\\ &\quad + g_{\mathrm{sk}}s_\infty([\mathrm{Ca}])(\xi_1+V_0-V_{\mathrm{K}})\\ &\quad + g_{\mathrm{bk}}f_\infty(\xi_1+V_0)(\xi_1+V_0-V_{\mathrm{K}})\\ &\quad + g_a a_\infty(\xi_1+V_0)(\xi_3+h_0)(\xi_1+V_0-V_{\mathrm{K}}).\end{aligned}$$

Consider the system

$$\dot{x} = Ax + F(x),\ x \in R^3,$$

where $A = A|_H$, $F(x)$ is a smooth vector function and $F(x) = O(\|x\|^2)$. $F(x)$ can be represented as

$$F(x) = \frac{1}{2}B(x,x) + \frac{1}{6}C(x,x,x) + O(\|x\|^4)$$

at the neighborhood of $x = 0$. Where $B(x, y)$ and $C(x, y, z)$ are multilinear vector functions, and $x = (x_1, x_2, x_3)^{\mathrm{T}}$, $y = (y_1, y_2, y_3)^{\mathrm{T}}$, $u = (u_1, u_2, u_3)^{\mathrm{T}}$.

Specifically, in coordinates, we have

$$B_i(x,y) = \sum_{j,k=1}^{3} \left.\frac{\partial^2 F_i(\xi)}{\partial\xi_j\partial\xi_k}\right|_{\xi=0} x_j y_k,\ i = 1,2,3,$$

$$C_i(x,y,u) = \sum_{j,k,l=1}^{3} \left.\frac{\partial^3 F_i(\xi)}{\partial\xi_j\partial\xi_k\partial\xi_l}\right|_{\xi=0} x_j y_k u_l,\ i = 1,2,3,$$

where $\xi = (\xi_1, \xi_2, \xi_3)^{\mathrm{T}}$.

Therefore, it is not complicated to compute

$$B(x, y) = \begin{pmatrix} -0.01773763x_1y_1 - 0.4(x_1y_2 + x_2y_1) \\ -5.09556659(x_1y_3 + x_3y_1) \\ 0.0000175305618x_1y_1 \\ 0.00000013749147x_1y_1 \end{pmatrix},$$

$$C(x, y, u) = \begin{pmatrix} -0.00044106463x_1y_1u_1 + \\ 0.01986145964(x_1y_1u_3 + x_1y_3u_1 + x_3y_1u_1) \\ -0.0000016866559x_1y_1u_1 \\ -0.00000002749073x_1y_1u_1 \end{pmatrix}.$$

Appendix B

We can rewrite the system as follows:

$$\frac{\mathrm{d}X}{\mathrm{d}t} = F(X, \mu) = \begin{pmatrix} G_1(X, \mu) \\ G_2(X, \mu) \\ G_3(X, \mu) \\ G_4(X, \mu) \end{pmatrix},$$

where $X = (V, n, h, [\mathrm{Ca}])^{\mathrm{T}}$, $\mu = (g_{\mathrm{bk}}, g_{\mathrm{sk}})^{\mathrm{T}}$, and

$$G_1 = -\frac{1}{C_{\mathrm{m}}} F_0,$$

$$G_2 = \frac{\lambda}{\tau_n} [n_\infty(V) - n],$$

$$G_3 = \frac{1}{\tau_h} [h_\infty(V) - h],$$

$$G_4 = -f_c \{\alpha g_{\mathrm{Ca}} m_\infty(V)(V - V_{\mathrm{Ca}}) + k_c[\mathrm{Ca}]\},$$

where $m_\infty(V), n_\infty(V), s_\infty(V), f_\infty(V)$ and $a_\infty(V)$ are defined in the above content.

Consider the Taylor series of $F(X, \mu)$ around (X_0, μ_0) as follows:

$$\begin{aligned} F(X, \mu) = {} & DF(X_0, \mu_0)(X - X_0) \\ & + F_\mu(X_0, \mu_0)(\mu - \mu_0) \\ & + \frac{1}{2} D^2 F(X_0, \mu_0)(X - X_0, X - X_0) \\ & + F_{\mu X}(X_0, \mu_0)(\mu - \mu_0, X - X_0) + \cdots. \end{aligned}$$

Note

$$B \triangleq DF(X_0, \mu_0) = \begin{pmatrix} \frac{\partial G_1}{\partial V} & \frac{\partial G_1}{\partial n} & \frac{\partial G_1}{\partial h} & \frac{\partial G_1}{\partial [\mathrm{Ca}]} \\ \frac{\partial G_2}{\partial V} & \frac{\partial G_2}{\partial n} & \frac{\partial G_2}{\partial h} & \frac{\partial G_2}{\partial [\mathrm{Ca}]} \\ \frac{\partial G_3}{\partial V} & \frac{\partial G_3}{\partial n} & \frac{\partial G_3}{\partial h} & \frac{\partial G_3}{\partial [\mathrm{Ca}]} \\ \frac{\partial G_4}{\partial V} & \frac{\partial G_4}{\partial n} & \frac{\partial G_4}{\partial h} & \frac{\partial G_4}{\partial [\mathrm{Ca}]} \end{pmatrix}.$$

We can calculate the eigenvalues of matrix B, which are 0, 0, −0.05001538536, 0.6355118804. Next, we will assume that $p_1, p_2 \in R^4$ are generalized eigenvectors that correspond to zero eigenvalue of B. Let $P = (p_1, p_2, P_0)$ be an invert matrix, which satisfies

$$P^{-1} B P = \begin{pmatrix} J_0 & 0 \\ 0 & J_1 \end{pmatrix},$$

where

$$J_0 = \begin{pmatrix} 0 & 1 \\ 0 & 0 \end{pmatrix}, \; J_1 = \begin{pmatrix} -0.05001538536 & 0 \\ 0 & 0.635511804 \end{pmatrix}.$$

Then, we can get

$$\begin{aligned} p_1 = {} & (1, 0.02494561460, -0.000002774149057, \\ & -0.0008235181936)^{\mathrm{T}}, \\ p_2 = {} & (1, -1.044151560, 0.00005270876537, \\ & 0.5138753283)^{\mathrm{T}}, \end{aligned}$$

$$P_0 = \begin{pmatrix} -45.83929075 & 1131.884357 \\ 1 & 1 \\ -0.4130569636 & -0.0002290327697 \\ -0.001247557576 & -0.002340951714 \end{pmatrix}.$$

Let $P^{-1} = (q_1, q_2, Q_0{}^{\mathrm{T}})^{\mathrm{T}}$; then, we can obtain

$$\begin{aligned} q_1 = {} & (-0.03925640296, 44.67205297, 112.2320192, \\ & 90.83474535)^{\mathrm{T}}, \\ q_2 = {} & (-0.00005872864288, 0.07140905060, \\ & 0.1730808461, 2.091191031)^{\mathrm{T}}, \end{aligned}$$

$$Q_0 = \begin{pmatrix} -0.0000002529718183 & 0.0009182064663 \\ -0.0002689868114 & -0.03954095832 \\ -2.421295828 & -0.1973782337 \\ -0.0002976805699 & -0.08211049236 \end{pmatrix}^{\mathrm{T}}.$$

Therefore, we can calculate the following expressions.

$$\begin{aligned} a = {} & \frac{1}{2} p_1{}^{\mathrm{T}} \left(q_2 \cdot D^2 F(X_0, \mu_0)\right) p_1 \\ = {} & 1.75568328184171 \times 10^{-6}, \\ b = {} & p_1{}^{\mathrm{T}} \left(q_1 \cdot D^2 F(X_0, \mu_0)\right) p_1 \\ & + p_1{}^{\mathrm{T}} \left(q_2 \cdot D^2 F(X_0, \mu_0)\right) p_2 \\ = {} & 0.00486009518308801, \\ S_1 = {} & F_\mu{}^{\mathrm{T}}(X_0, \mu_0) q_2 \\ = {} & (0.0003936532486, 0.0002998262570)^{\mathrm{T}}, \\ S_2 = {} & \left[\frac{2a}{b}\left(p_1{}^{\mathrm{T}} \left(q_1 \cdot D^2 F(X_0, \mu_0)\right) p_2\right.\right. \end{aligned}$$

$$
\begin{aligned}
&+ p_2{}^{\mathrm{T}}\left(q_2 \cdot D^2F(X_0,\mu_0)\right)p_2\Big)\\
&- p_1{}^{\mathrm{T}}\left(q_2 \cdot D^2F(X_0,\mu_0)\right)p_2\Big]F_\mu{}^{\mathrm{T}}(X_0,\mu_0)q_1\\
&-\frac{2a}{b}\sum_{i=1}^{2}\Big(q_i \cdot \Big(F_{\mu X}(X_0,\mu_0) - ((P_0\ J_1{}^{-1}Q_0)\\
&\times F_\mu(X_0,\mu_0))^{\mathrm{T}} \times D^2F(X_0,\mu_0)\Big)\Big)p_i\\
&+\Big(q_2 \cdot \Big(F_{\mu X}(X_0,\mu_0) - ((P_0\ J_1{}^{-1}Q_0)\\
&\times F_\mu(X_0,\mu_0))^{\mathrm{T}} \times D^2F(X_0,\mu_0)\Big)\Big)p_1\\
&= (-4.705762294\times 10^{-6}, -7.22688775)^{\mathrm{T}}.
\end{aligned}
$$

We can make the transformation $\lambda_1 = g_{\mathrm{bk}} + 12.645060$, $\lambda_2 = g_{\mathrm{sk}} - 15.956173$, that is, λ_1, λ_2 become a pair of bifurcation parameter. Then, we have

$$
\begin{aligned}
\beta_1 &= S_1{}^{\mathrm{T}}(\mu-\mu_0)\\
&= 0.0003.936532486\lambda_1 + 0.0002998262570\lambda_2,\\
\beta_2 &= S_2{}^{\mathrm{T}}(\mu-\mu_0)\\
&= -4.705762294\times 10^{-6}\lambda_1 - 7.22688775\lambda_2.
\end{aligned}
$$

Obviously, our nonlinear system conforms to the condition of Theorem 1 in [43]. By the theoretical methods, the dynamics on the center manifold of the whole system at $X = X_0$, $\mu = \mu_0$ is locally topologically equivalent to

$$
\begin{aligned}
\frac{\mathrm{d}z_1}{\mathrm{d}t} &= z_2,\\
\frac{\mathrm{d}z_2}{\mathrm{d}t} &= \beta_1 + \beta_2 z_1 + a{z_1}^2 + bz_1z_2\\
&= 0.0003936532486\lambda_1 + 0.0002998262570\lambda_2\\
&\quad +\Big(-4.705762294\times 10^{-6}\lambda_1\\
&\quad -7.22688775\lambda_2\Big)z_1\\
&\quad +1.75568328184171\times 10^{-6}{z_1}^2\\
&\quad +0.00486009518308801 z_1z_2.
\end{aligned}
$$

Making the replacement of variables by

$$
t = \left|\frac{b}{a}\right| t_1 = \left|\frac{0.00486009518308801}{0.00000175568328184171}\right| t_1,
$$

$$
\begin{aligned}
z_1 &= \frac{a}{b^2}\eta_1 = \frac{0.00000175568328184171}{(0.00486009518308801)^2}\eta_1,\\
z_2 &= \mathrm{sign}\left(\frac{b}{a}\right)\frac{a^2}{b^3}\eta_2\\
&= \frac{(0.00000175568328184171)^2}{(0.00486009518308801)^3}\eta_2.
\end{aligned}
$$

The original system becomes

$$
\begin{aligned}
\frac{\mathrm{d}\eta_1}{\mathrm{d}t_1} &= \eta_2,\\
\frac{\mathrm{d}\eta_2}{\mathrm{d}t_1} &= \bar{\beta}_1 + \bar{\beta}_2\eta_1 + {\eta_1}^2 + s\eta_1\eta_2,
\end{aligned}
$$

where

$$
\begin{aligned}
\bar{\beta}_1 &= \frac{b^4}{a^3}\beta_1\\
&= 4.05839597\times 10^4\lambda_1 + 3.091079973\times 10^4\lambda_2,\\
\bar{\beta}_2 &= \frac{b^2}{a^2}\beta_2\\
&= -36.06012167\lambda_1 - 5.537943388\times 10^7\lambda_2,\\
s &= \mathrm{sign}(ab) = 1.
\end{aligned}
$$

By the theory in [41], we can calculate the following equivalence term in advance.

$$
\begin{aligned}
&4\bar{\beta}_1 - \bar{\beta}_2^2 = 0\\
&\Leftrightarrow 0.0080101374 08{\lambda_1}^2 + 2.460318237\times 10^4\lambda_1\lambda_2\\
&+1.889220347\times 10^{10}{\lambda_2}^2 - \lambda_1 - 0.7616506608\lambda_2 = 0,\\
&\bar{\beta}_1 = 0\\
&\Leftrightarrow \lambda_1 = -0.7616506608\lambda_2,\\
&\bar{\beta}_2 < 0\\
&\Leftrightarrow \lambda_1 < -1.535752829\times 10^6\lambda_2,\\
&\bar{\beta}_1 + \frac{6}{25}\bar{\beta}_2^2 = o\left(\bar{\beta}_2^2\right)\\
&\Leftrightarrow 0.007689731910{\lambda_1}^2 + 2.361905508\times 10^4\lambda_1\lambda_2\\
&+1.813651533\times 10^{10}{\lambda_2}^2 + \lambda_1 + 0.7616506608\lambda_2\\
&= o\left(\|(\lambda_1,\lambda_2)\|^2\right).
\end{aligned}
$$

See Tables 1, 2.

Table 1 Parameter values are used in the calculation

Definition	Parameter values
Maximal conductances (nS)	$g_{\mathrm{ca}} = 2.0$, $g_{\mathrm{k}} = 4.0$, $g_{\mathrm{a}} = 25$
Time constants (ms)	$\tau_n = 30$, $\tau_h = 20$
Reversal potentials (mV)	$V_{\mathrm{Ca}} = 50$, $V_{\mathrm{K}} = -75$
Gating variable parameters (mV)	$V_m = -20$, $s_m = 12$, $V_n = -5$, $s_n = 10$, $V_f = -20$, $s_f = 5.6$, $V_{\mathrm{a}} = -20$, $s_a = 10$, $V_h = -60$, $s_h = 5$
Other parameters	$\lambda = 0.7$, $k_s = 0.5\mu\mathrm{M}$, $k_c = 0.16\mathrm{ms}^{-1}$, $f_c = 0.01$, $\alpha = 0.0015\mu MfC^{-1}$

Table 2 Data related to special points

Points	Coordinate values (g_{bk}, g_{sk})	Eigenvalues	Normal form coefficient
GH_1	(0.000703, − 48.975903)	$\lambda_{1,2} = \pm 0.0265214\mathrm{i}$, $\lambda_3 = -0.0500039$, $\lambda_4 = 0.20376$	$l_2 = -2.124141 \times 10^{-4}$
GH_2	(0.005693, − 37.067576)	$\lambda_{1,2} = \pm 0.0754509\mathrm{i}$, $\lambda_3 = -0.0500045$, $\lambda_4 = 0.0197066$	$l_2 = -6.945405 \times 10^{-4}$
GH_3	(0.014912, − 9.199701)	$\lambda_{1,2} = \pm 0.122114\mathrm{i}$, $\lambda_3 = -0.0500111$, $\lambda_4 = -0.000852519$	$l_2 = -5.108963 \times 10^{-5}$
GH_4	(0.011299, − 0.321252)	$\lambda_{1,2} = \pm 0.106296\mathrm{i}$, $\lambda_3 = -0.0501872$, $\lambda_4 = -0.00176338$	$l_2 = -4.991566 \times 10^{-6}$
GH_5	(0.000887, − 0.208443)	$\lambda_{1,2} = \pm 0.0297757\mathrm{i}$, $\lambda_3 = -0.0697144$, $\lambda_4 = -0.0149915$	$l_2 = -2.392979 \times 10^{-7}$
CP_1	(− 3.665138, 1.171912)	$\lambda_1 = 0$, $\lambda_2 = -0.239172$, $\lambda_3 = -0.049999$, $\lambda_4 = -0.0290647$	$c = -3.203405 \times 10^{-6}$
CP_2	(− 14.741551, 18.745219)	$\lambda_1 = 0$, $\lambda_2 = -0.0500106$, $\lambda_3 = 0.0283496$, $\lambda_4 = 0.273392$	$c = 1.372069 \times 10^{-5}$
CP_3	(− 2.264354, 3.503469)	$\lambda_1 = 0$, $\lambda_2 = -0.0502939$, $\lambda_3 = -0.011844$, $\lambda_4 = 0.54639$	$c = 9.359168 \times 10^{-6}$
HH_1	(0.003019, − 44.777990)	$\lambda_{1,2} = \pm 0.0549442\mathrm{i}$, $\lambda_{3,4} = \pm 0.0500042$,	None
HH_2	(− 0.000242, − 1.895243)	$\lambda_{1,2} = \pm 0.0573209$, $\lambda_{3,4} = \pm 0.0155559$,	None
ZH_0	(− 14.666964, 18.643160)	$\lambda_1 = 0$, $\lambda_{2,3} = \pm 0.05001$, $\lambda_4 = 0.183805$	None
ZH	(− 13.162279, 16.546031)	$\lambda_1 = 0$, $\lambda_{2,3} = \pm 0.116936\mathrm{i}$, $\lambda_4 = -0.0500084$	$(\mathrm{s}, \theta, E_0) = (1, -1.710129 \times 10^2, -1)$
BT	(− 12.645060, 15.956172)	$\lambda_{1,2} = 0$, $\lambda_3 = -0.0500154$, $\lambda_4 = 0.635512$	$(a, b) = (-2.018350 \times 10^{-7}, -5.211393 \times 10^{-3})$
$R2$	(− 0.7738865, 1.359544)	$\mu_1 = 0.063181$, $\mu_2 = 0.999998$, $\mu_{3,4} = 1$, $Arg_{1,2} = 0$, $Arg_{3,4} = 180.$	$(a, b) = (-2.264819 \times 10^{-7}, -1.071368 \times 10^{-4})$

References

1. Nunemaker, C.S., Straume, M., Defazio, R.A., Moenter, S.M.: Gonadotropin-releasing hormone neurons generate interacting rhythms in multiple time domains. Endocrinology **144**(3), 823–831 (2003)
2. Stojilkovic, S.S., Zemkova, H., Van, G.F.: Biophysical basis of pituitary cell type-specific Ca^+ signaling–secretion coupling. Trends Endocrinol. Metab. **16**(4), 152–159 (2005)
3. Tabak, J., Toporikova, N., Freeman, M.E., Bertram, R.: Low dose of dopamine may stimulate prolactin secretion by increasing fast potassium currents. J. Comput. Neurosci. **22**, 211–222 (2007)
4. Toporikova, N., Tabak, J., Freeman, M.E., Bertram, R.: A-type K^+ current can act as a trigger for bursting in the absence of a slow variable. Neural Comput. **20**(2), 436–451 (2008)
5. Tsaneva-Atanasova, K., Sherman, A., Van, G.F., Stojilkovic, S.S.: Mechanism of spontaneous and receptor-controlled electrical activity in pituitary somatotrophs: experiments and theory. J. Neurophysiol. **98**, 131–144 (2007)
6. Kuryshev, Y.A., Childs, G.V., Ritchie, A.K.: Corticotropin-releasing hormone stimulates Ca^+ entry through L- and P-type Ca^+ channels in rat corticotropes. Endocrinology **137**(6), 2269–2277 (1996)
7. Lebeau, A.P., Robson, A.B., Mckinnon, A.E., Sneyd, J.: Analysis of a reduced model of corticotroph action potentials. J. Theor. Biol. **192**, 319–339 (1998)
8. Shorten, P.R., Robson, A.B., Mckinnon, A.E., Wall, D.J.: CRH-induced electrical activity and calcium signalling in pituitary corticotrophs. J. Theor. Biol. **206**, 395–405 (2000)
9. Stern, J.V.: Resetting behavior in a model of bursting in secretory pituitary cells: distinguishing plateaus from pseudo-plateaus. Bull. Math. Biol. **70**, 68–88 (2008)
10. Rinzel, J.: A formal classification of bursting mechanisms in excitable systems. In: E. Teramoto, M. Yamaguti (Eds.), Mathematical Topics in Population Biology, Morphogenesis, and Neurosciences. Lecture Notes in Biomathematics, vol. 71, pp. 267–281. Springer, New York (1987)
11. Bertram, R., Butte, M.J., Kiemel, T., Sherman, A.: Topological and phenomenological classification of bursting oscillations. Bull. Math. Biol. **57**, 413–439 (1995)
12. Izhikevich, E.M.: Neural excitability, spiking, and bursting. Int. J. Bifurc. Chaos **10**, 1171–1266 (2000)
13. Izhikevich, E.M.: Dynamical Systems in Neuroscience: the Geometry of Excitability and Bursting. MIT Press, Cambridge (2007)
14. Izhikevich, E.M., Hoppensteadt, F.: Classification of bursting mappings. Int. J. Bifurc. Chaos **14**(11), 3847–3854 (2011)
15. Yang, Z., Lu, Q.: Different types of bursting in Chay neuronal model. Sci. China Ser. G **51**(6), 687–698 (2008)
16. Lu, B., Liu, S., Liu, X.: Bifurcation and spike adding transition in Chay–Keizer model. Int. J. Bifurc. Chaos **26**(05), 1650090 (2016)
17. Wang, J., Lu, B., Liu, S., Jiang, X.: Bursting types and bifurcation analysis in the Pre-Bötzinger complex respiratory rhythm neuron. Int. J. Bifurc. Chaos **27**(01), 231–245 (2017)
18. Liu, X., Liu, S.: Codimension-two bifurcation analysis in two-dimensional Hindmarsh–Rose model. Nonlinear Dyn. **67**(1), 847–857 (2012)
19. Huang, C., Sun, W., Zheng, Z., Lu, J., Chen, S.: Hopf bifurcation control of the M–L neuron model with type I. Nonlinear Dyn. **87**(2), 755–766 (2017)
20. Fan, D., Hong, L., Wei, J.: Hopf bifurcation analysis in synaptically coupled HR neurons with two time delays. Nonlinear Dyn. **62**(1), 305–319 (2010)
21. Zhao, Z., Jia, B., Gu, H.: Bifurcation and enhancement of neuronal firing induced by negative feedback. Nonlinear Dyn. **86**(3), 1–12 (2016)
22. Ma, J., Wu, F., Ren, G., Tang, J.: A class of initials-dependent dynamical systems. Appl. Math. Comput. **298**, 65–76 (2017)
23. Zhan, F., Liu, S.: Response of electrical activity in an improved neuron model under electromagnetic radiation and noise. Front. Comput. Neurosci. **11**, 107 (2017)
24. Lv, M., Wang, C., Ren, G., Ma, J., Song, X.: Model of electrical activity in a neuron under magnetic flow effect. Nonlinear Dyn. **85**(3), 1479–1490 (2016)
25. Li, J., Liu, S., Liu, W., Yu, Y., Wu, Y.: Suppression of firing activities in neuron and neurons of network induced by electromagnetic radiation. Nonlinear Dyn. **83**(1–2), 801–810 (2016)
26. Wechselberger, M.: Existence and bifurcation of canards in R^3 in the case of a folded node. Siam J. Appl. Dyn. Syst. **4**(1), 101–139 (2005)
27. Wechselberger, M., Weckesser, W.: Bifurcations of mixed-mode oscillations in a stellate cell model. Phys. D **238**(16), 1598–1614 (2009)
28. Wechselberger, M., Mitry, J., Rinzel, J.: Canard theory and excitability. Lect. Notes Math. **21**(02), 89–132 (2013)
29. Desroches, M., Guckenheimer, J., Krauskopf, B., Kuehn, C., Osinga, H.M., Wechselberger, M.: Mixed-mode oscillations with multiple time scales. Siam Rev. **54**(2), 211–288 (2012)
30. Brøns, M., Krupa, M., Wechselberger, M.: Mixed mode oscillations due to the generalized canard phenomenon. Fields Inst. Commun. **49**(1), 39–63 (2006)
31. Vo, T., Bertram, R., Tabak, J., Wechselberger, M.: Mixed mode oscillations as a mechanism for pseudo-plateau bursting. J. Comput. Neurosci. **28**(23), 443–458 (2010)
32. Vo, T., Bertram, R., Wechselberger, M.: Multiple geometric viewpoints of mixed mode dynamics associated with pseudo-plateau bursting. Siam J. Appl. Dyn. Syst. **12**(2), 789–830 (2013)
33. Vo, T., Bertram, R., Wechselberger, M.: A geometric understanding of how fast activating potassium channels promote bursting in pituitary cells. J. Comput. Neurosci. **36**(2), 259–278 (2014)
34. Teka, W., Tabak, J., Vo, T., Wechselberger, M., Bertram, R.: The dynamics underlying pseudo-plateau bursting in a pituitary cell model. J. Math. Neurosci. **1**(1), 12 (2011)
35. Dhooge, A., Govaerts, W., Kuznetsov, Y.A.: MATCONT: a MATLAB package for numerical bifurcation analysis of ODEs. ACM Trans. Math. Softw. **29**, 141–164 (2003)
36. Dhooge, A., Govaerts, W., Kuznetsov, Y.A., Mestrom, W., Riet, A.M., Sautois, B.: MATCONT and CL MATCONT: continuation toolboxes in MATLAB. Utrecht University, Utrecht (2006)

37. Rubin, J., Wechselberger, M.: Giant squid-hidden canard: the 3D geometry of the Hodgkin Huxley model. Biol. Cybern. **97**, 5–32 (2007)
38. Lu, B., Liu, S., Jiang, X., Wang, J., Wang, X.: The mixed mode oscillations in AV-RON-PARNAS-SEGEL model. Discrete Contin. Dyn. Syst. Ser. S **10**(3), 487–504 (2017)
39. Wechselberger, M.: Apropos canards. Trans. Am. Math. Soc. **364**, 3289–3309 (2012)
40. Teka, W., Tsaneva-Atanasova, K., Bertram, R., Tabak, J.: From plateau to pseudo-plateau bursting: making the transition. Bull. Math. Biol. **73**(6), 1292 (2011)
41. Kuznetsov, Y.A.: Elements of Applied Bifurcation Theory. Springer, New York (1998)
42. Guckenheimer, J., Holmes, P.: Nonlinear Oscillations, Dynamical Systems and Bifurcations of Vector Fields. Springer, New York (1983)
43. Carrillo, F.A., Verduzco, F., Delgado, J.: Analysis of the Takens–Bogdanov bifurcation on m-parameterized vector fields. Int. J. Bifurc. Chaos **20**, 995–1005 (2010)